Electronic Supplementary Information for

Syntheses and photophysical properties of new iminopyrrolyl boron complexes and their application in efficient single-layer non-doped OLEDs prepared by spin coating

D. Suresh,[a] Clara S. B. Gomes,[a] Pedro T. Gomes,*[a] Roberto E. Di Paolo,[a]
António L. Maçanita,[a] Maria José Calhorda,[b] Ana Charas,[c] Jorge Morgado,[c,d]
and M. Teresa Duarte[a]

[a] *Centro de Química Estrutural, Departamento de Engenharia Química, Instituto Superior Técnico, Universidade Técnica de Lisboa, Av. Rovisco Pais, 1049-001 Lisboa, Portugal*

[b] *Departamento de Química e Bioquímica, CQB, Faculdade de Ciências, Universidade de Lisboa, Campo Grande, Ed. C8, 1749-016 Lisboa, Portugal*

[c] *Instituto de Telecomunicações, Av. Rovisco Pais, 1049-001 Lisboa, Portugal*

[d] *Departamento de Bioengenharia, Instituto Superior Técnico, Universidade Técnica de Lisboa, Av. Rovisco Pais, 1049-001 Lisboa, Portugal*

Experimental section

General

All experiments dealing with air- and/or moisture-sensitive materials were carried out under inert atmosphere using a dual vacuum/nitrogen line and standard Schlenk techniques. Nitrogen gas was supplied in cylinders by specialized companies (e.g., Air Liquide, etc.) and purified by passage through 4 Å molecular sieves. Unless otherwise stated, all reagents were purchased from commercial suppliers (e.g., Acros, Aldrich, Fluka) and used without further purification. All solvents to be used under inert atmosphere were thoroughly deoxygenated and dehydrated before use. They were dried and purified by refluxing over a suitable drying agent followed by distillation under nitrogen. The following drying agents were used: sodium (for toluene), calcium hydride (for hexane and dichloromethane). Solvents and solutions were transferred using a positive pressure of nitrogen through stainless steel cannulae and mixtures were filtered in a similar way using modified cannulae that could be fitted with glass fiber filter disks. The ligand precursors IminopyrrH-Ph (**1**), $(\text{IminopyrrH})_2$-1,4-Ph (**2**), $(\text{IminopyrrH})_2$-4,4′-biphenyl (**3**) and BPh_3 were prepared and characterized according to the literature methods.[1,2]

Nuclear magnetic resonance (NMR) spectra were recorded on Bruker Avance III 300 (^1H, ^{13}C, and ^{11}B) spectrometer. Deuterated solvents were dried by storage over 4 Å molecular sieves and degassed by the freeze-pump-thaw method. Spectra were referenced internally using the residual proton solvent resonance relative to tetramethylsilane (δ=0) for ^1H. All chemical shifts are quoted in δ (ppm) and coupling constants given in Hertz. Multiplicities were abbreviated as follows: broad (br), singlet (s), doublet (d), triplet (t), quartet (q), heptet (h), and multiplet (m). For air- and/or moisture sensitive materials, samples were prepared in J. Young tubes in glovebox. Elemental analyses were obtained from the IST elemental analysis services.

General procedure for the syntheses of complexes 4 - 6

A mixture of triphenylboron and the appropriate stoichiometric amount of the desired IminopyrrH-R ligand precursor in 15-25 mL toluene were heated to reflux under nitrogen atmosphere overnight (16 - 20 h). The reaction mixture was brought to room temperature and then concentrated under vacuum to 5 mL and double layered with hexane. The resulting solution was kept at -20 °C to afford the corresponding crystalline boron complexes.

BPh_2(Iminopyrr-Ph) (4). In the same manner as described above, a mixture of 0.100 g (0.58 mmol) of IminopyrrH-Ph (**1**) and 0.142 g (0.58 mmol) of BPh_3 afforded BPh_2(Iminopyrr-Ph) as a yellow solid. Yield: 0.154 g (80%). The crystals suitable for single crystal X-ray diffraction studies were obtained by double layering of the compound with toluene and hexane and kept at -20 °C. ^{1}H NMR (300 MHz, CD_2Cl_2): δ_H 8.40 (s, 1H, C*H*=N), 7.29-7.20 (m, 15H, B*Ph₂+phenyl*), 7.19-7.18 (m, 1H, *pyrr*), 7.02 (dd, $^3J_{HH}$ = 3.9 Hz, $^4J_{HH}$ = 0.9 Hz, 1H, *pyrr*), 6.56 (dd, $^3J_{HH}$ = 3.9 Hz, $^4J_{HH}$ = 1.8 Hz, 1H, *pyrr*). ^{13}C NMR (75 MHz, CD_2Cl_2): δ_C 150.6, 147.6, 142.1, 134.3, 133.1, 131.3, 129.2, 127.5, 127.3, 126.6, 122.1, 117.2, 115.0. ^{11}B NMR (96.3 MHz, CD_2Cl_2): δ_B 4.89. Anal. Calcd (%) for $C_{23}H_{19}BN_2$: C, 82.65; H, 5.73; N, 8.38. Found: C, 82.26; H, 5.63; N, 8.15. This compound has a wavelength of the first vibronic emission transition (λ_{em}^{0-0}) at 451 nm, an emission maximum at 478 nm and the fluorescence quantum yield is 34 %.

Ph_2B(Iminopyrr-1,4-Ph-Iminopyrr)BPh_2 (5). In the same manner as described above, a mixture of 0.120 g (0.50 mmol) of $(IminopyrrH)_2$-1,4-Ph (**2**) and 0.242 g (1.00 mmol) of BPh_3 afforded Ph_2B(Iminopyrr-1,4-Ph-Iminopyrr)BPh_2 as a yellow solid. Yield: 0.238 g (81%). The crystals suitable for single crystal X-ray diffraction studies were obtained by keeping the dichloromethane solution of the compound at -20 °C. ^{1}H NMR (300 MHz, CD_2Cl_2): δ_H 8.42(s, 2H, C*H*=N), 7.17 (s, 22 H, B*Ph$_2$+pyrr*), 7.15 (s, 4H, *phenyl*), 7.02 (d, J_{HH} = 4.2 Hz, 2H, *pyr*), 6.53 (dd, $^3J_{HH}$ = 4.2 Hz, $^4J_{HH}$ = 2.1 Hz, 2H, *pyrr*). ^{13}C NMR (75 MHz, CD_2Cl_2): δ_C 150.0, 145.8, 140.8, 134.5, 133.2, 131.9, 127.7, 126.8, 122.7, 117.8, 115.7. ^{11}B NMR (96.3 MHz, CD_2Cl_2): δ_B 5.48. Anal. Calcd (%) for $C_{40}H_{32}B_2N_4$ C, 81.38; H, 5.46; N, 9.49. Found: C, 81.28; H, 5.11; N, 8.95. This compound has a wavelength of the first vibronic emission transition (λ_{em}^{0-0}) at 512 nm, which is coincident the emission maximum, and the fluorescence quantum yield is 69 %.

Ph_2B(Iminopyrr-4,4′-biphenyl-Iminopyrr)BPh_2 (6). In the same manner as described above, a mixture of 0.200 g (0.59 mmol) of $(IminopyrrH)_2$-4,4′-biphenyl (**3**) and 0.286 g (1.18 mmol) of BPh_3 afforded Ph_2B(Iminopyrr-4,4′-biphenyl-Iminopyrr)BPh_2 as a yellow solid. Yield: 0.346 g (86%). ^{1}H NMR (300 MHz, CD_2Cl_2): δ_H 8.60 (s, 2H, C*H*=N), 7.50 (d, 9Hz 4 H, *phenyl*), 7.38-7.20 (m, 26H, B*Ph$_2$+phenyl+pyrr*), 7.09 (dd, $^3J_{HH}$ = 3.9 Hz, $^4J_{HH}$ = 0.9 Hz, 2H, *pyrr*), 6.60 (dd, $^3J_{HH}$ = 3.9 Hz, $^4J_{HH}$ = 1.8 Hz, 2H, *pyrr*). ^{13}C NMR (75 MHz, CD_2Cl_2): δ_C 149.9, 141.4, 138.4, 134.4, 133.1, 131.5, 128.1, 127.5, 127.4, 126.6, 122.3, 117.4, 115.3. ^{11}B NMR (96.3 MHz, CD_2Cl_2): δ_B 3.90. Anal. Calcd (%) for $C_{46}H_{36}B_2N_4$ C, 82.90; H, 5.44; N, 8.41. Found: C, 82.45; H, 5.30; N, 8.16. This compound has a wavelength of the first vibronic emission transition (λ_{em}^{0-0}) at 497 nm, an emission maximum at 531 nm and the fluorescence quantum yield is 64 %.

X-Ray data collection

Crystallographic and experimental details of crystal structure determinations are listed in Table 1. The crystals were selected under an inert atmosphere, covered with polyfluoroether oil, and mounted on a nylon loop. Crystallographic data for compounds **4** and **5** were collected using graphite monochromated Mo-Ka radiation (λ =0.71073 Å) on a Bruker AXS-KAPPA APEX II diffractometer equipped with an Oxford Cryosystem open-flow nitrogen cryostat, at 150 K. Cell parameters were retrieved using Bruker SMART software and refined using Bruker SAINT on all observed reflections. Absorption corrections were applied using SADABS.[3] Structure solution and refinement were performed using direct methods with the programs SIR2004[4] and SHELXL[5] both included in the package of programs WINGX-Version 1.80.05.[6] Except for the N*H* hydrogen atoms in compounds, all hydrogen atoms were inserted in idealised positions and allowed to refine riding on the parent carbon atom.

Table S1. Crystallographic data for compounds **4** and **5**

	4	**5**
formula	$C_{23}H_{19}BN_2$	$C_{40}H_{32}B_2N_4 \cdot 2CH_2Cl_2$
M	334.22	760.17
λ /Å	0.71073	0.71073
T / K	150	150
crystal system	Monoclinic	Monoclinic
space group	C2/c (No. 15)	P 21/n
a /Å	17.7637(16)	8.1967(3)
b/Å	11.2623(10)	11.7901(4)
c / Å	18.0062(15)	19.9616(6)
α / deg	90	90.00
β /deg	90.691(5)	95.809(2)
γ / deg	90	90.00
V / Å^3	3602.1(5)	1919.18(11)
Z	8	2
ρcalc /g cm^{-3}	1.233	1.315
crystal size mm^{-1}	0.20 × 0.20 × 0.40	0.30 × 0.40 × 0.60
θ_{max} / deg	26.6	25.75
total data	15888	21705
unique data	3696	3654
R_{int}	0.041	0.034
R [I > 2σ(I)]	0.0397	0.0509
wR	0.1060	0.1340
gooodness of fit	1.037	1.062
ρ min, ρ max	-0.22, 0.23	-0.62, 0.67

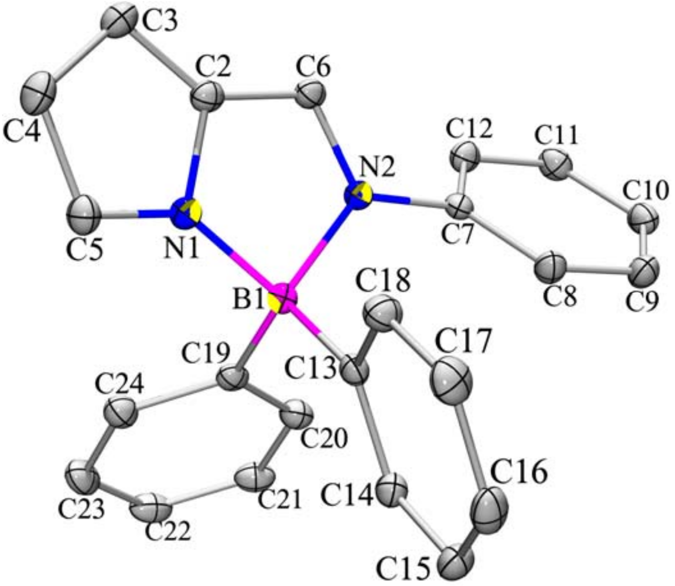

Figure S1. Perspective view of molecular structure of **4**. The ellipsoids were drawn at 30% probability level. All the hydrogen atoms were omitted for clarity. Selected bond lengths (Å): N1-C2, 1.3757(17); N1-C5, 1.3466(17); N2-C6, 1.3088(16); N2-C7, 1.4324(16); N1-B1, 1.5687(18); N2-B1, 1.6327(19); C19-B1, 1.619 (2); C13-B1, 1.6112(19). Selected bond angles (°):N1-B1-N2, 94.95(10); N1-B1-C13, 110.56(11); N1-B1-C19, 112.05(11); N2-B1-C13, 111.88(10); N2-B1-C19, 110.00(10); C13-B1-C19, 115.56(11); C2-N1-C5, 107.67(11); C2-N1-B1, 112.21(11); C5-N1-B1, 140.00(12).

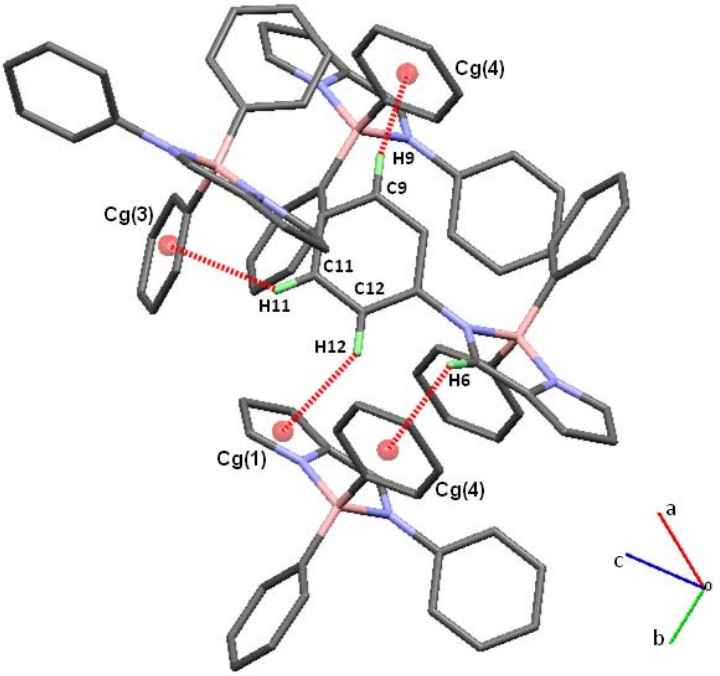

Figure S2. Crystal packing of **4** showing C–H···π interactions (C6–H6···Cg(4), symmetry operation 1/2-x,1/2-y,1-z; C9–H9···Cg(4), symmetry operation 1-x,-y,1-z; C11–H11···Cg(3), symmetry operation x,-y,1/2+z; C12–H12···Cg(1), symmetry operation 1/2-x,1/2-y,1-z), which are depicted by dashed lines.

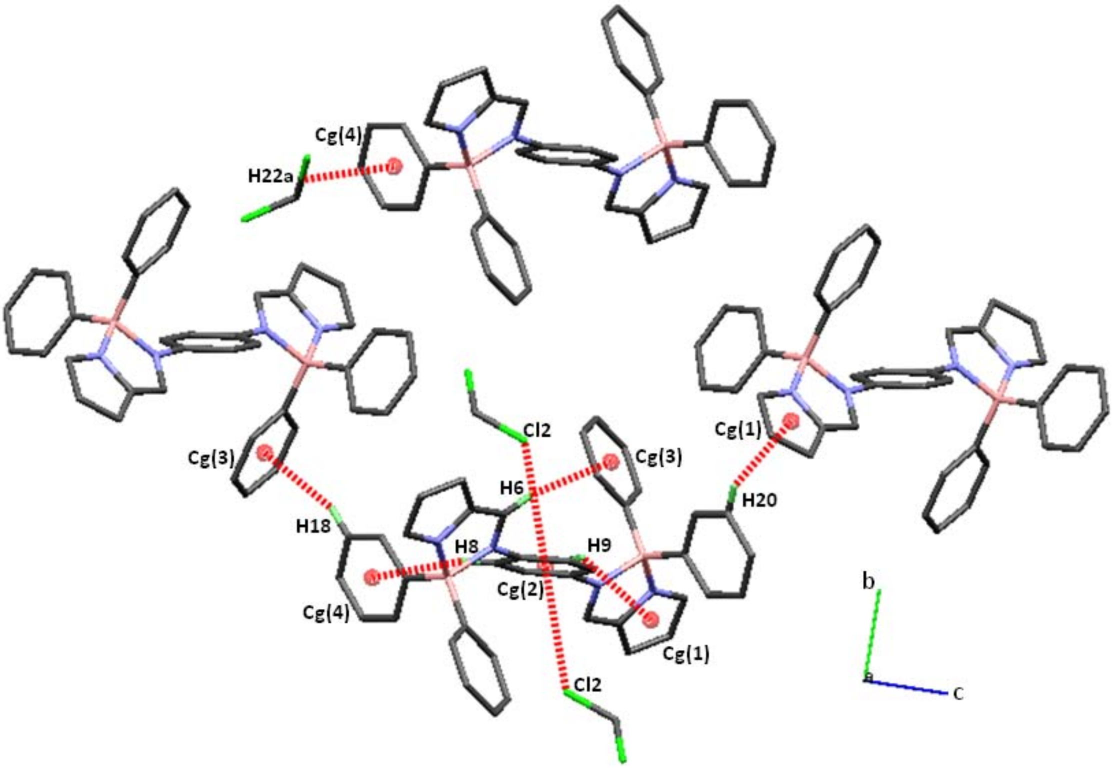

Figure S3. Crystal packing of **5** showing C–H···π interactions (C6–H6···Cg(3), symmetry operation -x,-y,2-z; C8–H8···Cg(4), symmetry operation x,y, z; C9–H9···Cg(1), symmetry operation -x,-y,2-z; C18–H18···Cg(3), symmetry operation 1/2-x,1/2+y,3/2-z; C20–H20···Cg(1), symmetry operation 1/2-x,-1/2+y,3/2-z; C22–H22A···Cg(4), symmetry operation 1+x,1+y,z) and C–Cl···π (C22–Cl2···Cg(2), symmetry operation 3/2-x,1/2+y,3/2-z; C22–Cl2···Cg(2), symmetry operation 1/2+x,1/2-y,-1/2+z), represented by dashed lines, viewed along the *a* axis.

Spectroscopic measurements

Absorption spectra were measured on a Beckman DU-70 spectrophotometer. Solution fluorescence spectra were measured on a SPEX Fluorolog 212I, at the right angle geometry. The same instrument was used to obtain the thin film fluorescence (or photoluminescence, PL) spectra of the complexes, which were prepared on spectrosil discs by spin coating from THF solutions. The photoluminescence spectra were collected in the S/R mode and corrected for instrumental wavelength dependence. Fluorescence decays were measured using the picosecond time-correlated single-photon counting (TCSPC) technique, as previously described.[7] The experimental FWHM of the excitation pulse was 18 ps. Global analyses of fluorescence decays were carried out with the Sand program.[7]

Fluorescence decays of complexes 4-6

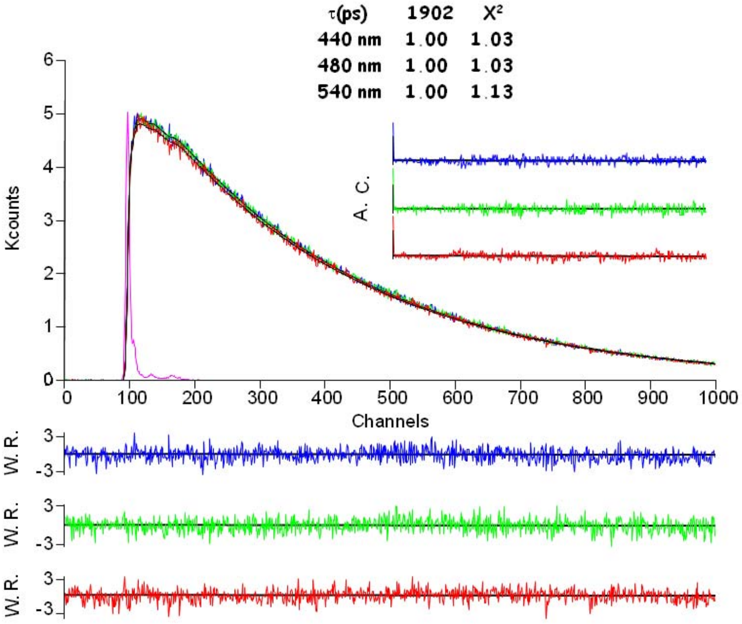

Figure S4. Global analysis of fluorescence decays of **4** in THF, at 293 K, measured at three emission wavelengths (440, 480 and 540 nm), with excitation at 400 nm. The decay times and pre-exponential coefficients at each emission wavelength are indicated in the figure. The weighted residuals (W.R.), autocorrelation functions (A.C.), and χ^2 values are also shown. The excitation pulse is the narrowest one shown in magenta. The data were collected with 6.1 picoseconds per channel.

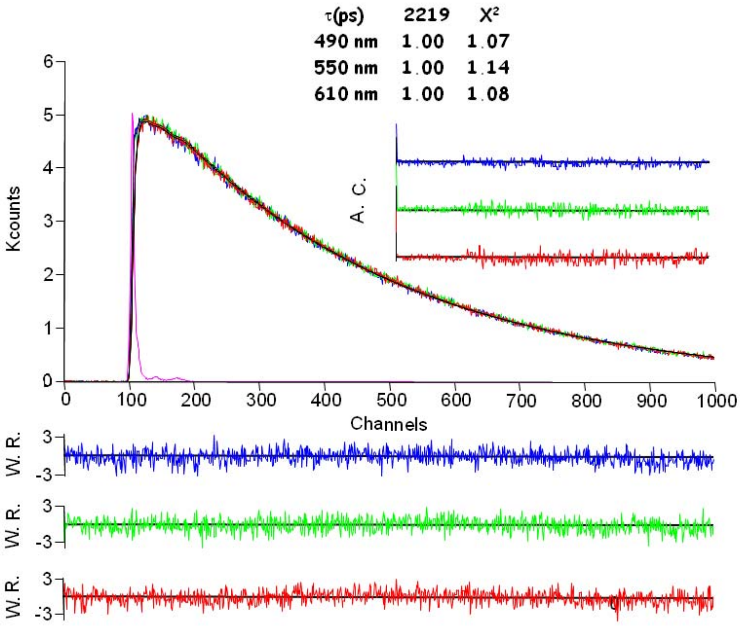

Figure S5. Global analysis of fluorescence decays of **5** in THF, at 293 K, measured at three emission wavelengths (490, 550 and 610 nm), with excitation at 440 nm. The decay times and pre-exponential coefficients at each emission wavelength are indicated in the figure. The data were collected with 6.1 picoseconds per channel.

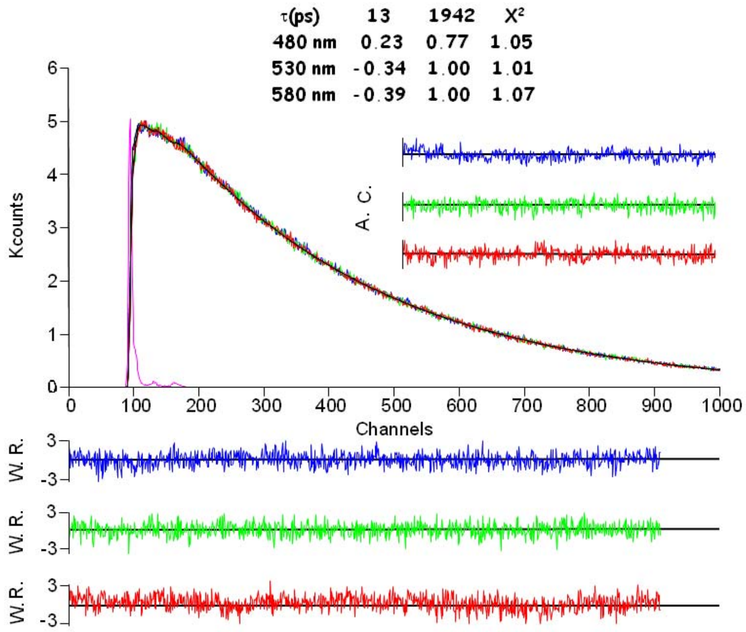

Figure S6. Global analysis of fluorescence decays of **6** in THF, at 293 K, measured at three emission wavelengths (480, 530 and 580 nm), with excitation at 440 nm. The data were collected with 6.1 picoseconds per channel. The shortest time component is a decay at the band onset (480 nm) and a rise-time at longer wavelengths.

Computational studies

All Density Functional Theory calculations[8] were performed using the Amsterdam Density Functional program package (ADF).[9] Gradient corrected geometry optimisations,[10] without symmetry constraints, were performed using the Local Density Approximation of the correlation energy (Vosko-Wilk-Nusair),[11] and the Generalised Gradient Approximation (Becke's exchange[12] and Perdew's correlation functionals).[13] Relativistic effects were treated with the ZORA approximation.[14] Unrestricted calculations were performed for excited singlet states. The core orbitals were frozen for B, C, and N (1s). Triple ζ Slater-type orbitals (STO) were used to describe the valence shells B, C, and N (2s and 2p). A set of two polarization functions was added to B, C, and N (single ζ, 3d, 4f). Triple ζ Slater-type orbitals (STO) were used to describe the valence shells of H (1s) augmented with two polarization functions (single ζ, 2s, 2p). Time Dependent DFT calculations in the ADF implementation were performed to determine the excitation energies.[15] The structures were modelled after those of compounds **4** and **5** described in this work. Three-dimensional representations of the orbitals were obtained with Molekel[16] and electronic spectra with Chemcraft.[17]

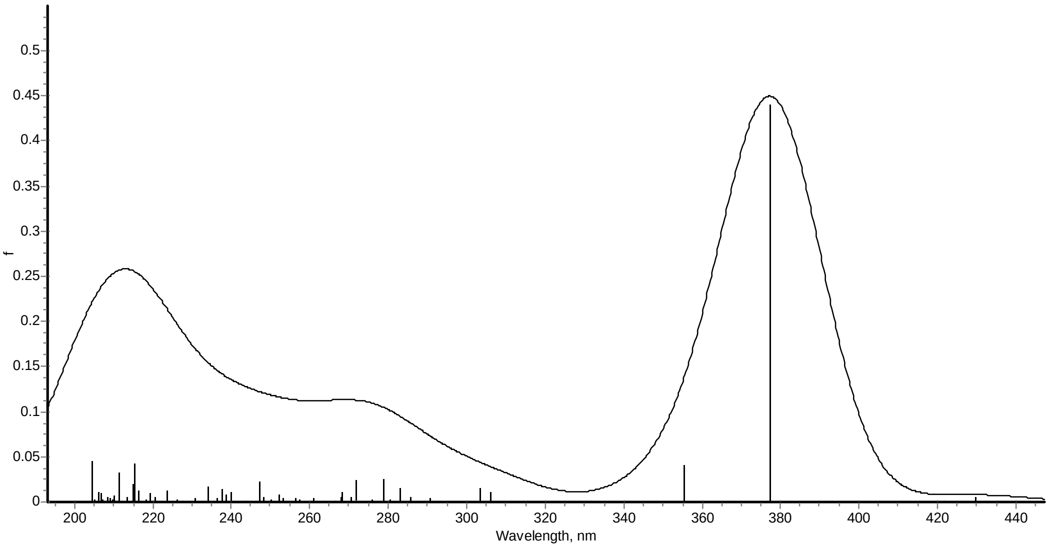

Figure S7. Calculated absorption spectrum of **4**, with a maximum at 377 nm.

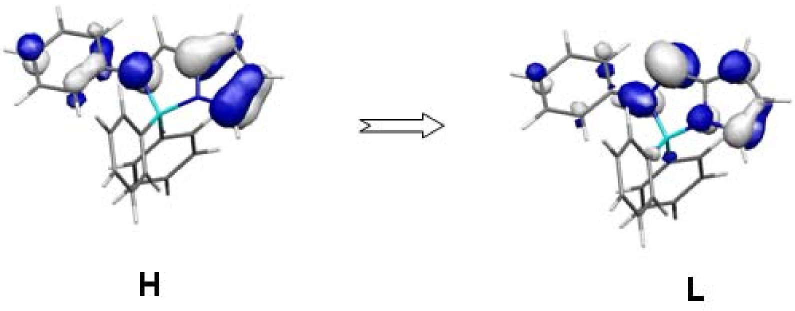

Figure S8. The orbitals of **4** involved in the electronic transition at 377 nm.

Cyclic voltammetry studies

In order to determine the ionization potential and electron affinity of the complexes **4-6** we performed cyclic voltammetry. The measurements were carried out using a standard 3-electrodes cell, using a saturated calomel reference electrode, a platinum wire as counter electrode and a platinum disk as working electrode, with a Solartron potentiostat. The compounds were dissolved in freshly distilled dichloromethane containing 0.2 M tetrabutylammonium tetrafluorborate as electrolyte. Figure S9 compares the voltammograms obtained for the three compounds at a scan rate of 50 mV/s. While the reduction is irreversible for the three compounds, the oxidation may be considered as being partially reversible.

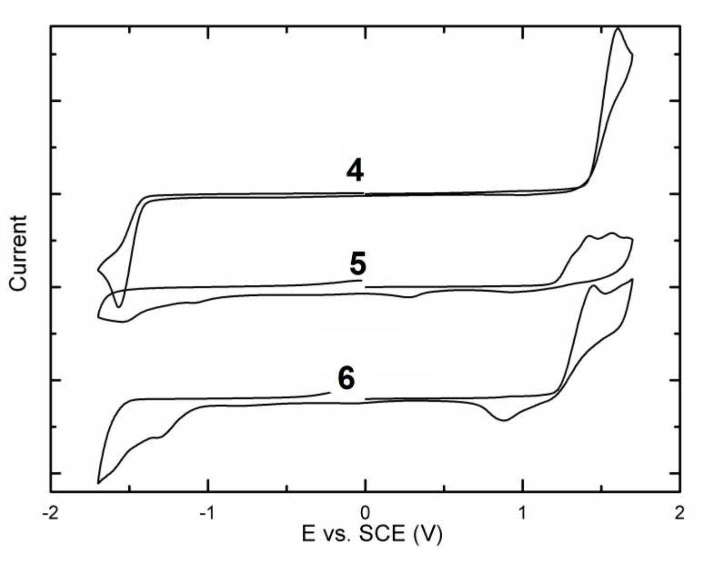

Figure S9. Voltammograms of complexes **4-6**.

We have used the onset oxidation and reduction potentials to estimate the ionization potential and the electron affinity, respectively.[18] To convert the values of the electrochemical scale into the absolute one, referred to vacuum, we consider that the energy level of ferrocene/ferrocenium

(Fc/Fc$^+$) is at 4.80 eV below the vacuum level.[19] The half-wave potential determined under these experimental conditions for Fc/Fc$^+$ is 0.57 V. Therefore, we calculate IP (eV)= E_{ox}^{on}(V)+4.23 and EA(eV)=E_{red}^{on}(V)+4.23.

Light-emitting diodes

Light-emitting diodes were prepared on glass/ITO substrates, which were cleaned with detergent, distilled water, acetone and isopropanol. They were treated with oxygen plasma, prior to the deposition of PEDOT:PSS (CLEVIOS P VP.AI 4083 from Heraeus Clevios GmbH) by spin coating. The PEDOT:PSS films (40 nm thick, as measured with a DEKTAK profilometer) were annealed in air for 2 minutes at 120 ^oC, and then transferred into a glovebox. Films of the complexes **4** to **6** were deposited on top, by spin coating, from their THF solutions, prepared inside the glovebox. The substrates were then placed inside an evaporation chamber, and the top metal cathodes (barium or calcium), ca. 40 nm thick, were deposited at a base pressure of 2×10^{-6} mbar through a shadow mask, defining pixel areas of 4 mm^2. A protecting aluminium layer of ca. 60 nm thickness was deposited on top. We consider these devices as “single-layer” structures, as PEDOT:PSS acts as hole-injection layer, increasing the hole injection efficiency into the emissive layer. It acts as a metallic-like contact, as it also quenches the excitons if they are formed at its vicinity. This naming also intends to differentiate these structures from those with selective charge transporting and/or blocking effects.

Devices were tested under vacuum, using a K2400 Source Meter and a calibrated silicon photodiode, as described previously.[20] The electroluminescence (EL) spectra were obtained with a CCD spectrograph (from Ocean Optics or from ScanSci).

Figure S10 shows the characteristics of typical ITO/PEDOT:PSS/…/Ca/Al devices. Fig S11 compares the EL spectra with solution and thin films PL spectra for the three complexes. Fig.

S12 shows the energetic position of the relevant frontier levels of the various components used in the LEDs.

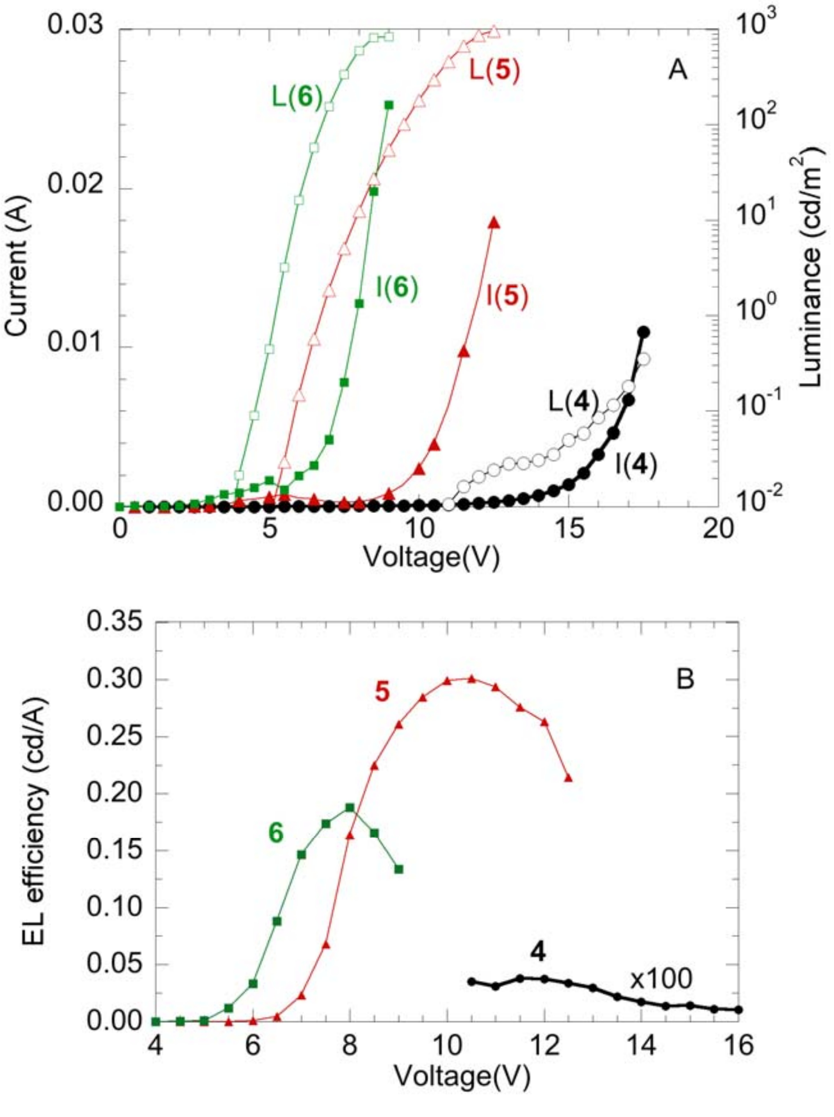

Figure S10. A) Current (I, filled symbols) and luminance (L, open symbols) of the devices based on complexes **4-6**. B) Corresponding EL efficiency. The thickness of the boron-complexes emissive layer is 90 nm for **4**, 80 nm for **5** and 60 nm for **6**.

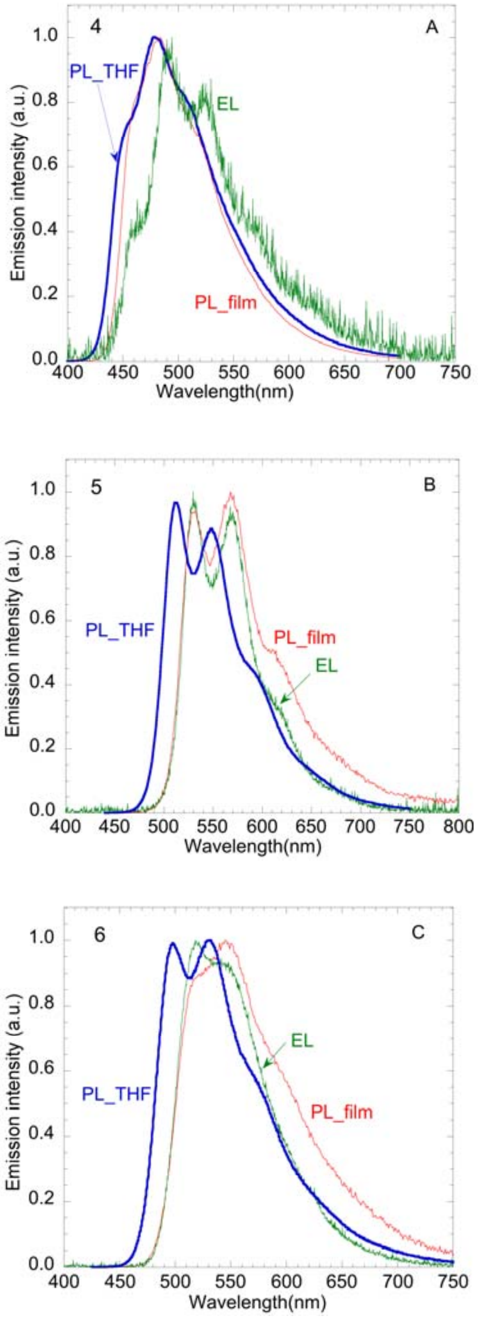

Figure S11. Comparison of solution and thin film PL spectra of the boron-complexes **4** to **6** with the corresponding EL spectra. While for **4** the solution and thin film PL spectra are similar, a small red-shift (ca. 20 nm) occurs in the PL of thin films of the other two complexes with respect to solution. The EL spectra, in particular for complexes **5** and **6**, are very similar to the solid state PL.

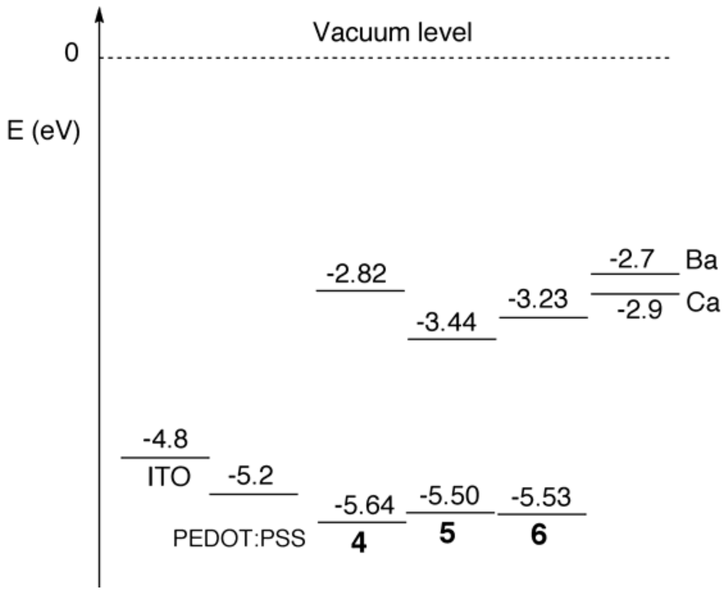

Figure S12. Energy level diagram of the components involved in the "single-layer" devices based on complexes **4**, **5** and **6**. The energies of complexes **4**, **5** and **6** are the experimental ones, derived from the cyclic voltammetry measurements. Based on this diagram, we note that no electron injection barrier is expected to exist between either Ca or Ba and the LUMOs of any of the three complexes. On the other hand, a small and similar hole-injection barrier is anticipated to exist between PEDOT:PSS and the HOMO of the three complexes.

We have not looked at structures that could maximise devices performance, as we intend to provide the characterisation of the simplest devices and to test these materials' ambipolarity and emission efficiency.

It should be mentioned that devices based on complexes **4** and **5** with 20% by weight of an oxadiazole (1,3-bis[(4-*tert*-butylphenyl)-1,3,4-oxidiazolyl]phenylene, OXD-7), known as a good electron-transporting molecule, with an ionization potential of 6.5 eV and an electron affinity EA=2.8 eV,[21] show higher values for the maximum EL efficiency (up to 0.16 cd A^{-1} for **4** and 0.67 cd A^{-1} for **5**) accompanied by a significant current decrease, which is likely due to electron trapping at the OXD-7 sites (though a much smaller effect is expected for complex **4**), thereby reducing the excess electron current within the emissive layer, as boron-complexes are reported to be good electron transporting materials.[22]

Complex **6** was also used in single-layer LEDs with barium cathodes. We find that the use of barium does not improve device performance, in spite of the fact that Ba is a better electron-injection contact than Ca, due to its lower workfunction (2.7 eV *vs* 2.9 eV for Ca). The current increases and the luminance slightly decreases, leading to a maximum EL efficiency of these Ba-based LEDs of ca. 0.13 cd A^{-1}. This result is again in agreement with the reported higher electron than hole mobility in boron-complexes. It is also consistent with the data in Figure S12, as using either Ca or Ba there should be no electron injection barrier.

References

1. (a) S. A. Carabineiro, L. C. Silva, P. T. Gomes, L. C. J. Pereira, L. F. Veiros, S. I. Pascu, M. T. Duarte, S. Namorado and R. T. Henriques, *Inorg. Chem.*, 2007, **46**, 6880–6890. (b) C. Pozo-Gonzalo, J. A. Pomposo, J. Rodríguez, E. Y. Schmidt, A. M. Vasil'tsov, N. V. Zorina, A. V. Ivanov, B. A. Trofimov, A. I. Mikhaleva and A. B. Zaitsev, *Synthetic Met.*, 2007, **157**, 60–65.

2. R. Köster, P. Binger and W. Fenzl, *Inorg. Synth.*, 1974, **15**, 134–136.

3. G. M. Sheldrick, 1996. *SADABS*. University of Göttingen, Germany.

4. M. C. Burla, R. Caliandro, M. Camalli, B. Carrozzini, G. L. Cascarano, L. De Caro, C. Giacovazzo, G. Polidori and R. Spagna, *J. Appl. Cryst.*, 2005, **38**, 381–388.

5. G. M. Sheldrick, *Acta Cryst.*, 2008, **A64**, 112–122.

6. L. J. Farrugia, *J. Appl. Cryst.*, 1999, **32**, 837–838.

7. R. E. Di Paolo, H. D. Burrows, J. Morgado and A. L. Maçanita, *ChemPhysChem.*, 2009, **10**, 448–454.

8. R. G. Parr and W. Young, in *Density Functional Theory of Atoms and Molecules*, Oxford University Press, New York, 1989.

9. (a) ADF2009, SCM, Theoretical Chemistry, Vrije Universiteit, Amsterdam, The Netherlands, http://www.scm.com; (b) G. te Velde, F. M. Bickelhaupt, S. J. A. van Gisbergen, C. F. Guerra, E. J. Baerends, J. G. Snijders and T. Ziegler, *J. Comput. Chem.,* 2001, **22**, 931–967. (c) C. F. Guerra, J. G. Snijders, G. te Velde and E. J. Baerends, *Theor. Chem. Acc.,* 1998, **99**, 391–403.

10. (a) L. Versluis and T. Ziegler, *J. Chem. Phys*., 1988, **88**, 322–328; (b) L. Fan, T. Ziegler, *J. Chem. Phys*., 1991, **95***,* 7401–7408.

11. S. H. Vosko, L. Wilk and M. Nusair, *Can. J. Phys*., 1980, **58**, 1200–1211.

12. A. D. Becke, *J. Chem. Phys.* 1987, **88**, 1053–1062.

13. (a) J. P. Perdew, *Phys. Rev. B* 1986, **33**, 8822–8824; (b) J. P. Perdew, Phys. Rev. B 1986, **34**, 7406.

14. E. van Lenthe, A. Ehlers and E. J. Baerends, *J. Chem. Phys.* 1999, **110**, 8943–8953.

15. (a) S. J. A. van Gisbergen, J. G. Snijders and E. J. Baerends, *Comput. Phys. Commun.* 1999, **118**, 119–138. (b) A. Rosa, E. J. Baerends, S. J. A. van Gisbergen, E. van Lenthe, J. A. Groeneveld and J. G. Snijders, *J. Am. Chem. Soc.* 1999, **121**, 10356–10365. (c) F. Wang, T. Ziegler, *Mol. Phys.* 2004, **102**, 2585–2595.

16. S. Portmann and H. P. Lüthi, *Chimia* 2000, **54**, 766–770.

17. http://www.chemcraftprog.com/index.html.

18. A. Charas, J. Morgado, J. M. G. Martinho, L. Alcácer, S. F. Lim, R. H. Friend and F. Cacialli, *Polymer* 2003, **44**, 1843–1850.

19. J. Pommerehne, H. Vestweber, W. Guss, R. F. Mahrt, H. Bässler, M. Porsh and J. Daub, *Adv. Mater.,* 1995, **7**, 551–554.

20. J. Morgado, A. Charas, J. A. Fernandes, I. S. Gonçalves, L. D. Carlos and L. Alcácer , *J. Phys. D: Appl. Phys.*, 2006, **39**, 3582–3587.

21. F.-C. Chen, S.-C. Chien and Y.-S. Chen, *Appl. Phys. Lett.* , 2009, **94**, 043306.

22. C. Sun, Z. M. Hudson, M. G. Helander, Z.-H. Lu and S. Wang, *Organometallics*, 2011, **30**, 5552–5555.